JOURNAL OF PROPULSION AND POWER
Vol. 20, No. 1, January–February 2004

Approach to High-Performance Transonic Compressor Design

M. Oana,* O. Kawamoto,† H. Ohtani,‡ and Y. Yamamoto§
Honda R&D Co., Ltd., Saitama 351-0193, Japan

A single stage transonic centrifugal compressor for a small turbofan engine has been developed. Rig testing has demonstrated an 83.2% adiabatic efficiency with a 7.5:1 total-to-static pressure ratio and a corrected tip speed of 596 m/s. An impeller blade redesign is presented of the original blade geometry, which uses both experimental and numerical results. An in-house developed Navier–Stokes flow solver was applied to the impeller redesign process. To meet the development schedule, a steady flow solver was used for the impeller analysis instead of an unsteady stage analysis. As a result, the following important redesign factors for higher efficiency were found: leading-edge shock control, blade-to-blade loading control, and splitter-loading optimization. Also, the flow physics of a secondary flow mechanism was captured by the computational analysis, and its control was applied during the impeller redesign process. The final stage performance was achieved by rig testing, through use of a coupled pipe diffuser and impeller-inducer bleed system.

Nomenclature

G	=	mass flow rate, kg/s
gH	=	adiabatic specific work, J/kg
LP	=	loading parameter, $(W_{ss} - W_{ps})/[(W_{ss} + W_{ps})/2]$
N	=	rotational speed, rad/s
Ns	=	specific speed, $129 \times ns$
ns	=	$NQ^{1/2}(gH)^{-3/4}$
Q	=	volume flow rate, m^3/s
SM	=	surge margin, $1 - (\pi_{work}/\pi_{surge} \times G_{surge}/G_{work})$, %
W	=	relative flow velocity, m/s
η	=	stage adiabatic efficiency
π	=	stage total-to-static pressure ratio

Subscripts

bleed	=	inducer bleed
inlet	=	impeller inlet position
ps	=	pressure surface
ss	=	suction surface
surge	=	surge point
work	=	working point on operating line

Introduction

AT the end of 2000, the initial stage performance of a transonic centrifugal compressor for a small turbofan engine demonstrated a satisfactory level of the stage efficiency of 82.2%, using a splitter blade, a pipe diffuser, and an impeller-inducer bleed system. Subsequently, a new research program on the transonic centrifugal compressor was started to obtain an efficiency increase of 1%, without changing the stage total-to-static pressure ratio of 7.5. This was a requirement for further improving specific fuel consumption in the small turbofan engine.

Received 5 August 2002; revision received 5 May 2003; accepted for publication 7 May 2003.

*Assistant Chief Engineer, Research Laboratory 4, Wako Research Center, 1-4-1 Chuo, Wako; Mineyasu_Oana@n.f.rd.honda.co.jp. Member AIAA.

†Assistant Chief Engineer, Research Laboratory 1, Wako Research Center, 1-4-1 Chuo, Wako.

‡Assistant Chief Engineer, Research Laboratory 4, Wako Research Center, 1-4-1 Chuo, Wako.

§Engineer, Research Laboratory 4, Wako Research Center, 1-4-1 Chuo, Wako.

An additional effort based on numerical and experimental investigation was devoted to the redesign of the centrifugal compressor, focusing on the impeller redesign. For the experimental investigation, a conventional measurement system was used, and the impeller-inducer bleed system was also studied. Numerical simulations were routinely used during the redesign process. The computational fluid dynamics (CFD) code that was used did not always calculate the absolute values of the aerodynamic properties accurately. However, differences in aerodynamic characteristics of each different design were generally calculated accurately enough for redesign purposes.

As a result, a stage efficiency of 83.2% was successfully demonstrated. Figure 1 shows an efficiency trend curve for various single-stage centrifugal compressors. All of the data were obtained from Rodgers.[1] Figure 1 shows the results of his simplified efficiency prediction technique. It was found that the improved compressor compares favorably with the world's best.

The purpose of the present investigation is to provide aerodynamic guidelines for the redesign of a transonic impeller with splitter blades using results of the research program, which demonstrated of 1% efficiency increase. In the current study, numerical results are first compared with experimental data. Further numerical analysis is then used to explore possible design modifications for improved efficiency. Finally, the inducer-bleed system is discussed.

Experimental Method

Test Facility

The test facility for the centrifugal compressor is shown in Fig. 2. The test compressor is driven by a 700-kW dc motor coupled to a gearbox. The allowable maximum speed is 100,000 rpm. The mass flow rate was measured with the flow meter located downstream of the air intake and was controlled with the throttle valve downstream of the collector. A part of the flow aspirated by the compressor could be bled from slits installed in the impeller shroud. The primary and bleed mass flow were exhausted to atmospheric pressure, and it was also possible to change the bleed mass flow using suction from a vacuum pump. The bleed mass flow rate was measured with a venturi flow meter.

Instrumentation

Figure 3 shows the meridional cross section of the test rig with measurement planes. A reduced-scale rig was used. Instrumentation for the inlet flowfield consisted of three total pressure probes and two total temperature probes located upstream of an S-shaped duct.[2] Instrumentation for the exit flowfield of the compressor stage consisted of two static pressure taps at the collector exit and with three sheathed thermocouples in the collector.

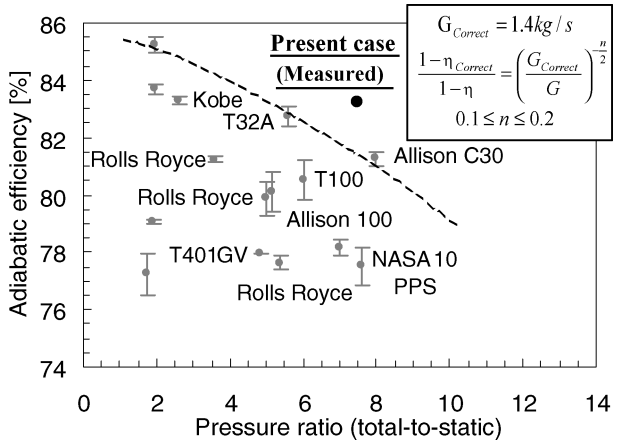

Fig. 1 Efficiency trend curve for single stage centrifugal compressors (from Rodgers[1]).

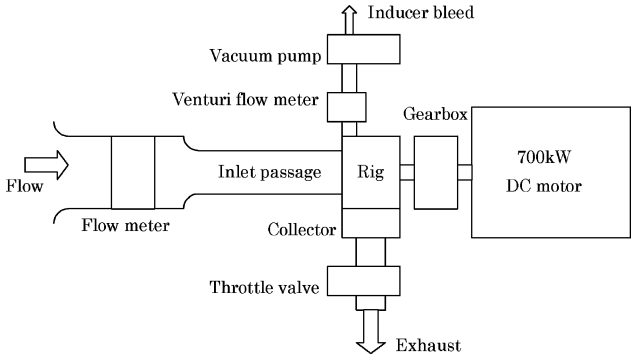

Fig. 2 Test facility for centrifugal compressor.

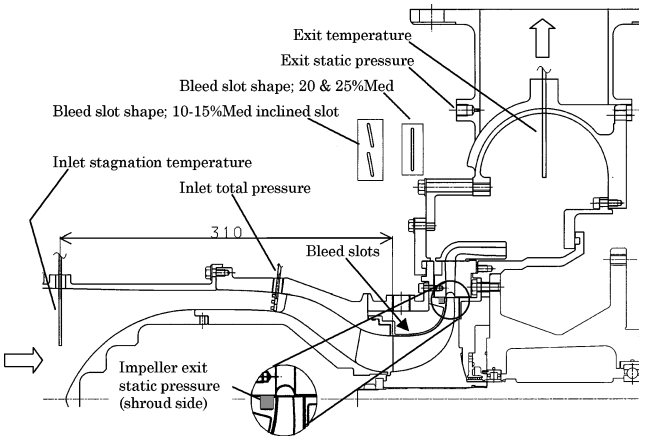

Fig. 3 Meridional cross section of test rig.

Measurement Accuracy

For the inlet, a DSA3016 pressure transducer with a range of 35 kPa(5 psid) was used, whereas for the collector exit, a transducer with a range of 700 kPa(100 psid) was used. The system accuracy was ±0.1% full scale. Differences in the measurements from the two static pressure taps at the collector exit were very small (±0.07%), corresponding to ±0.005 pressure ratio. A highly accurate temperature measurement system was used throughout, and by calibrating, the system accuracy was ±0.1°C at the inlet and ±0.2°C at the exit. Then, the accuracy of the calculated performance, that is, adiabatic efficiency, was ±0.1%. The repeatability was ±0.05% for a continuous testing and ±0.2% from day to day.

Fig. 4 Computational grid for impeller with splitter blades.

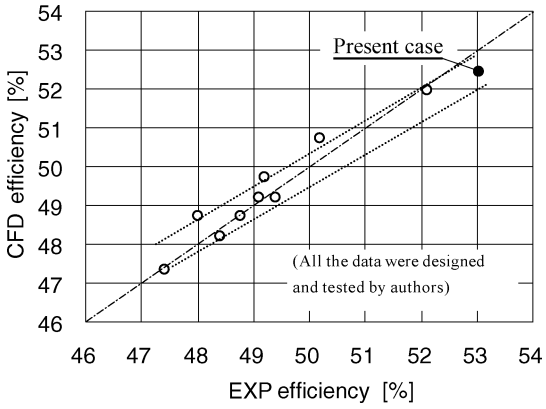

Fig. 5 Comparison of CFD with EXP on impeller total-to-static efficiency.

Computational Methods

A three-dimensional Navier–Stokes code with a low Reynolds number k–ε turbulence model[3] was applied to model the flow within the centrifugal compressor impeller and part of the S-shaped duct. An example of the computational body-fitted grid is shown in Fig. 4. Part of the casing grid is omitted to allow a better view of the impeller. The grid consisted of 49 × 2 nodes, which included two channels in the blade-to-blade direction, 49 nodes in the spanwise direction, and 196 nodes in the streamwise direction. For inlet boundary conditions, standard pressure and temperature were used, and an inlet flow without swirl was assumed.

Validation of the CFD code for a subsonic centrifugal compressor impeller with full blades had previously been conducted on Krain's impeller[4] using different turbulence models.[5] An additional validation was carried out for only the transonic impeller with splitter blades used in this investigation. Figure 5 shows the calculated and measured impeller total-to-static efficiency. To focus on the effect of some typical design parameters of the impeller geometry, many impellers were designed and tested. The experimental data (EXP) were obtained directly from static pressure taps located at impeller exit, without assuming a blockage factor.[4,6] That is the reason why the efficiency level is around 50%. It can be seen that the accuracy of the CFD code is sufficient for the redesign purpose, although there are quantitative differences.

Redesign Approach

From a detailed analysis using NASTRAN and the CFD code, it was found that there was one stress issue and three aerodynamic issues for the initial impeller with a 47.5-deg backsweep. The stress issue is high stress at exducer root due to high backsweep. The aerodynamic issues are 1) rapid acceleration and deceleration at the full blade leading edge (LE), 2) a strong three-dimensional

flowfield within the blades, and 3) an unbalanced flowfield at splitter passages.

Modification of One-Dimensional Design

To obtain both reliability and a 1% efficiency increment without changing the stage total-to-static pressure ratio, modifications to the one-dimensional design as well as the length of fillet R were made. The exit blade height and the fillet R around the exducer root were increased, while the backsweep was significantly increased. This appears to be a better compromise to achieve the goals of acceptable stress level, efficiency, and constant pressure ratio. The blade count was also changed from $15+15$ to $14+14$ to achieve a more acceptable balance between efficiency and surge margin. In our experience, a lower blade count gives better efficiency but lower surge margin. The final design specifications are listed in Table 1.

Modification of Aerodynamic Design

Key points for three aerodynamic issues listed earlier are as follows: 1) reduction of rapid acceleration and deceleration at LE of full blade, 2) reduction of hub loading parameter (LP), and 3) even split of mass flow at splitter LE. To achieve these aerodynamic goals, a new blade design approach was adopted. In the initial design, the camber angles were defined at two sections at the hub and tip. In the modified design, the blade camber angles are defined at multiple sections (five sections), and the blade half thicknesses of the suction surface (SS) and pressure surface (PS) are defined independently, instead of prescribing equal thicknesses for both sides.

In the following sections, the effects of these modifications on the flowfield are discussed.

Table 1 Typical design data for scaled compressor

Parameter	Value
Pressure ratio	
without S-shaped duct	7.5:1
with S-shaped duct	7.31:1
Corrected mass flow, kg/s	1.42
Corrected tip speed, m/s	596
Inducer bleed air, %	2.8
Blade number	$14+14$
Impeller tip radius, mm	95
Average blade exit angle, deg	49
Impeller exit passage height, mm	7.8
Fillet R at SS exit, mm	6.6
Specific speed, Ns	77
Relative tip inlet Mach number (average Mach number ahead of LE)	1.19

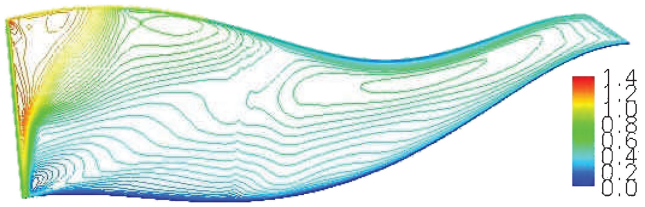

a) Initial impeller

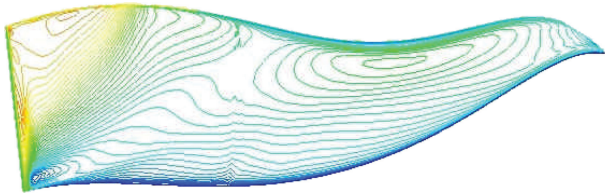

b) Improved impeller

Fig. 6 Mach number contours on the suction surface.

Results and Discussion

Reduction of Rapid Acceleration and Deceleratrion at LE of Full Blade

Figures 6a and 7a show Mach number contours on the full blade suction surface and at 50% span near the LE for the initial blade, respectively. It can be seen that there is a rapid acceleration and deceleration of the flow from hub to midspan near the LE, but the inlet Mach number is completely subsonic from hub ($M=0.65$) to midspan ($M=0.92$). This appears to lead to a large loss near the LE of the full blade.

To improve this pattern, the spanwise distribution of LE thickness and the LE wedge angle were modified, as shown in Figs. 8 and 9, respectively, using five blade sections instead of two. The blade thickness for the improved blade is decreased, especially in vicinity

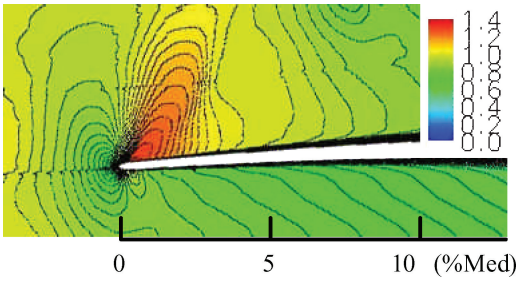

a) Initial impeller

b) Improved impeller

Fig. 7 Mach number contours near LE at midspan height.

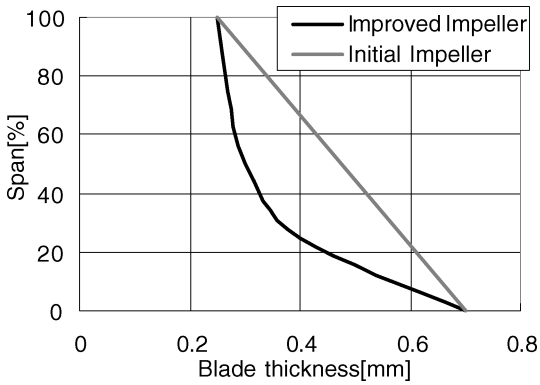

Fig. 8 Full blade spanwise thickness distribution at LE.

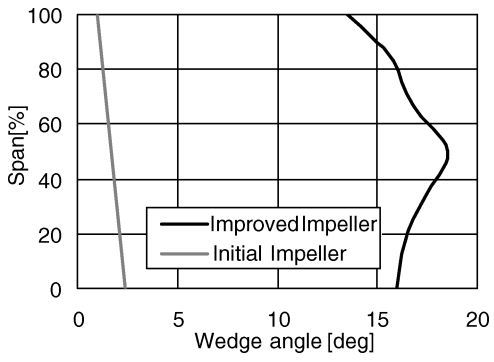

Fig. 9 Full blade spanwise wedge angle distribution at LE.

of 40% span compared with the same thickness at hub and tip in the initial impeller. Also, the wedge-in angle is significantly enlarged. It can be seen that there is a significant improvement of the flowfield near the LE on the full blade suction surface, as shown in Figs. 6b and 7b. The thickness redistribution was calculated to result in a 0.3% impeller efficiency increase.

Reduction of Hub Loading Parameter

A strong three-dimensional flow was observed within the blade passages. It is believed that the three-dimensional flow was mainly due to a secondary flow. A reduction of hub loading was studied to find the influence of this factor on the movement of low-momentum fluid.

There are several ways in which hub loading can be reduced. When the constraints of rake angle at the impeller exit, LE lean angle, and sufficient surge margin are considered, only the method of independent half-thickness distribution on the SS and PS already described in "Modification of Aerodynamic Design" could be used. In this case, only the suction side thickness was enlarged, as shown in Fig. 10. The improved impeller blade is thicker, and the curvature at about 50% of meridional position is more relaxed compared with the initial impeller at the hub. Spanwise, the added thickness is distributed without changing the blade tip thickness. Figure 11 shows a meridional distribution of the loading parameter at 20% span. It can be seen that the loading parameter (LP) is significantly decreased around the middle part of the impeller. Figure 12 shows a perspective view of the paths of CFD tracers released at 50% of meridional position close to the hub suction surfaces of the full and splitter blades, respectively. In comparison with the initial impeller, it can be seen that the low-momentum fluid on both blades (full and splitter) is more controlled at the exit of the improved impeller. Note that

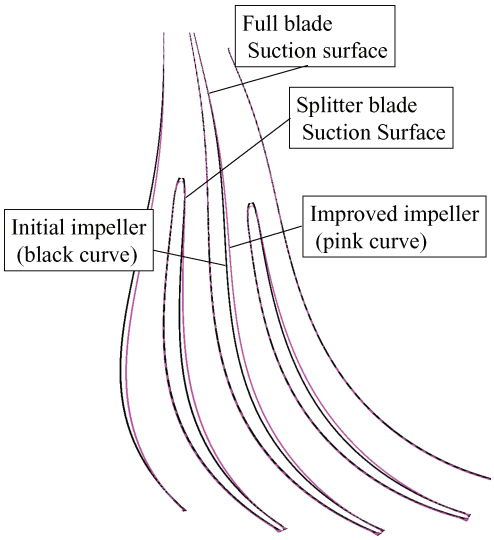

Fig. 10 Blade geometry differences between initial and improved impellers at hub section.

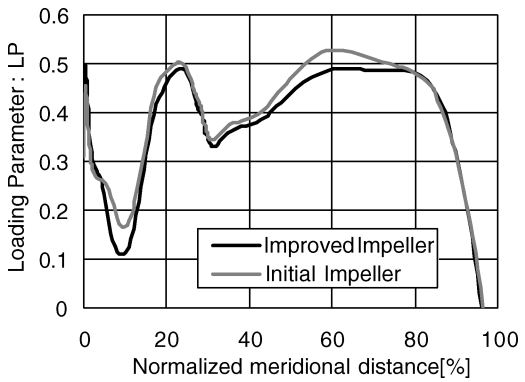

Fig. 11 LP at 20% span.

Table 2 Effect of mass flow split on efficiency for each passage

	Initial impeller		Improved impeller	
Passage	Flow rate, %	Efficiency, %	Flow rate, %	Efficiency, %
A	50.28	93.84	50.0	93.85
B	49.72	93.56	50.0	93.71

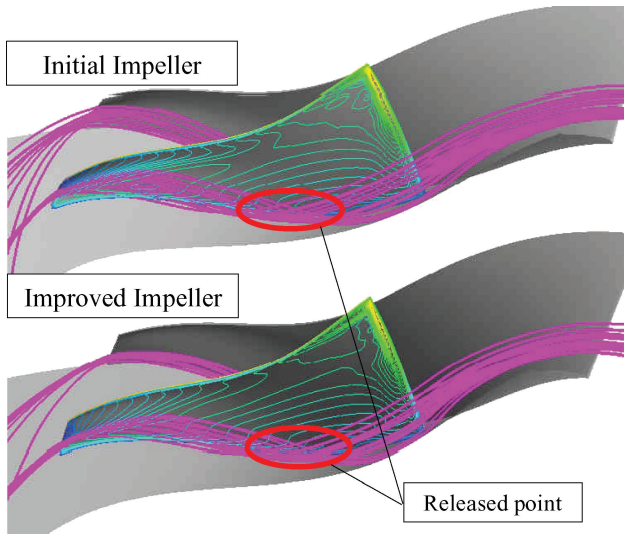

Fig. 12 Perspective view of path of CFD tracers near SS.

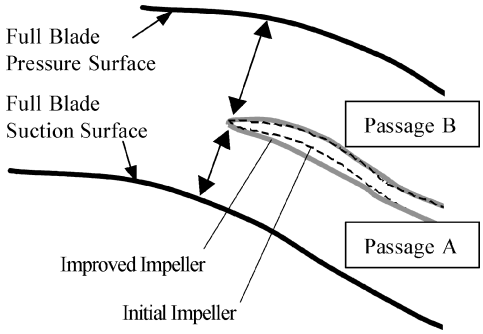

Fig. 13 Image view of geometry difference around splitter LE.

the Mach number contours on the suction side of splitter blade are significantly changed. Although the effect of the relaxation of hub loading on the impeller efficiency appears to be large, the CFD analysis indicates that that the efficiency increase is approximately 0.1%.

Even Split of Mass Flow at Splitter LE

Splitter blades located at midpitch of the full blade channel are usually used in the transonic centrifugal compressor impellers. The geometry is the same as that of the full blades except in the vicinity of the LE, where the splitters are thinner and rounded to avoid an acceleration in the relative frame. In this study, for the initial impeller, an incidence angle adjustment at the LE was implemented, as shown in Fig. 13 (dotted line). In Fig. 13, the geometry is exaggerated for illustrative purposes.

The same concepts that were used for modifying the initial impeller were also used for the improved impeller. For the initial impeller, a larger amount of low-momentum fluid and a higher entropy region were observed in passage B, adjacent to the pressure side of the full blade (shown later), resulting in an uneven split of mass flow between the two passages. Therefore, it was considered worthwhile to redesign the front section of the geometry of the splitter blade to have an even mass flow split, focusing on the flow incidence angle and the curvature of the pressure side.

As shown in Table 2, the calculated mass flow split for the initial impeller is 50.3:49.7. For the improved impeller, it is 50:50, resulting in an improved efficiency of about 0.15% for passage B only.

Although there is only a small difference in mass flow rate, it was found that the modification on the LE splitter blade was very important. The even split of mass flow resulted in an improvement overall in efficiency of approximately 0.1% for both passages A and B.

Performance Map

Calculated Impeller Performance

Figures 14a and 14b show calculated efficiency and total pressure ratio for the initial and the improved impellers, respectively. In this calculation, the fillet R is not simulated. An increase of the total pressure ratio is demonstrated. The increment of total pressure ratio is similar to what was estimated. The 1% efficiency increase was

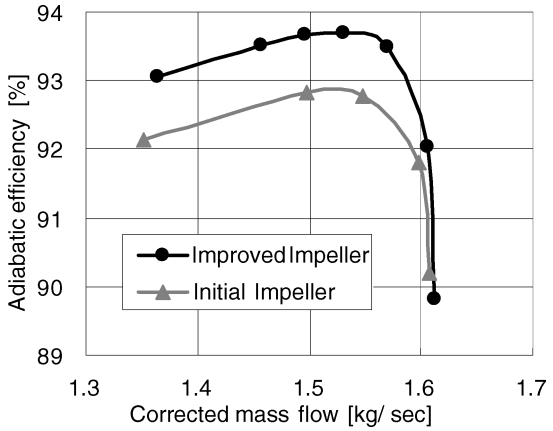

a) Adiabatic efficiency

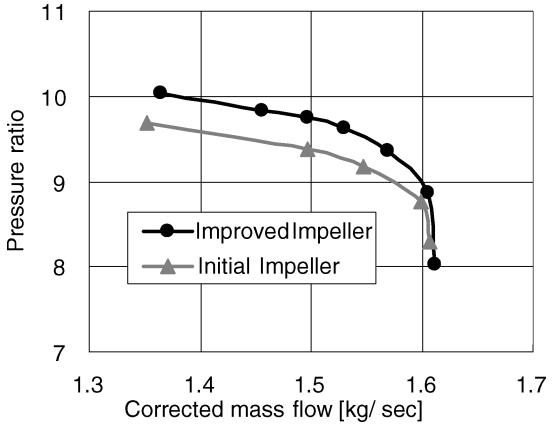

b) Total-to-total pressure ratio

Fig. 14 Calculated impeller performance map without fillet R.

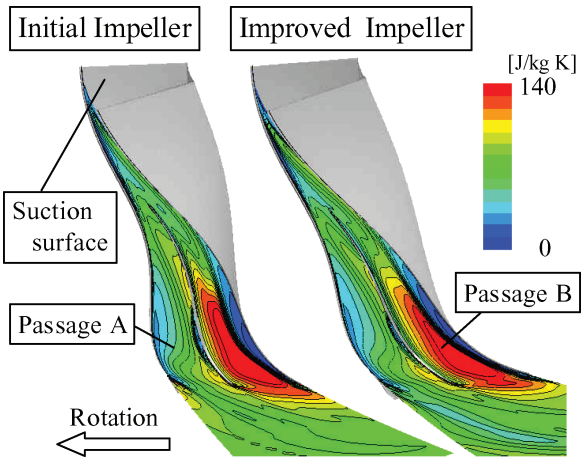

Fig. 15 Entropy pattern at 95% span height.

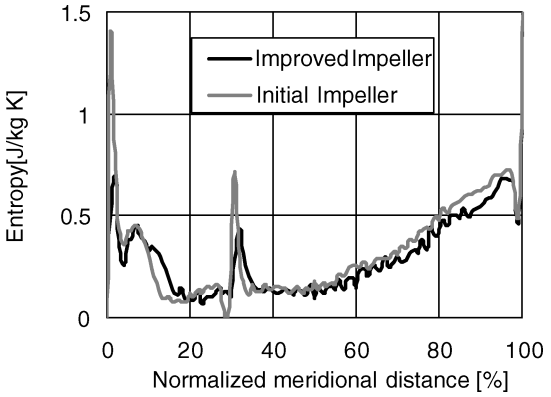

Fig. 16 Local entropy distribution along meridional direction.

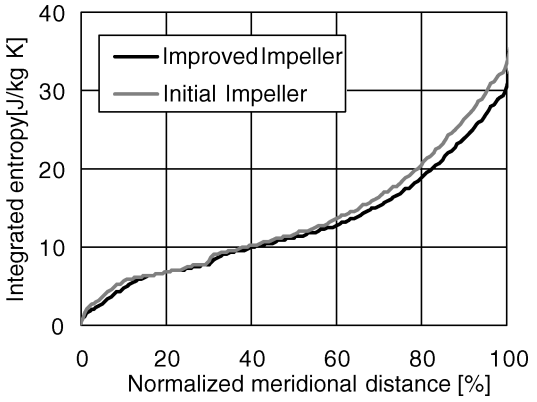

Fig. 17 Integrated entropy pattern along meridional direction.

obtained by the combination of the preceding three modifications and the reduction in blade count.

Figure 15 shows the comparison of entropy pattern at 95% span for the two impellers. As described earlier, there is a high loss region in passage B similar to that observed by Krain et al.[7] A significantly improved flowfield was obtained in the improved impeller compared with the initial impeller.

Figure 16 shows a comparison of the local entropy pattern along meridional direction for the initial and the improved impellers. The flowfield near the LE of the full and the splitter blades and close to the exducer is improved.

Figure 17 shows the comparison of the integrated entropy pattern for both impellers. The improved impeller has lower losses at the exit.

Experimental Stage Performance

The measured stage performance maps for both impellers are shown in Fig. 18 including normalized meridional distance from LE along the shroud line of the impeller (%Med). As already described, stage performance was measured with the S-shaped duct located upstream of the centrifugal compressor. The efficiency of the improved impeller was increased by approximately 1% while maintaining the same surge margin (SM). The total pressure ratio was approximately the same, which met engine requirements.

The demonstrated maximum efficiency was 82.7%. Because the S-shaped duct loss corresponds to a decrease of about 0.5% of the stage efficiency, the maximum efficiency without the S-shaped duct is expected to be 83.2%.

Effect of Inducer Bleed

In the stage performance tests, a target flow of 2.8% was bled from the inducer at the design point through a normal slot located at approximately 25% of the meridional length on the shroud surface. To investigate effects of bleed level and position on stage performance in more detail, an additional experiment has been carried

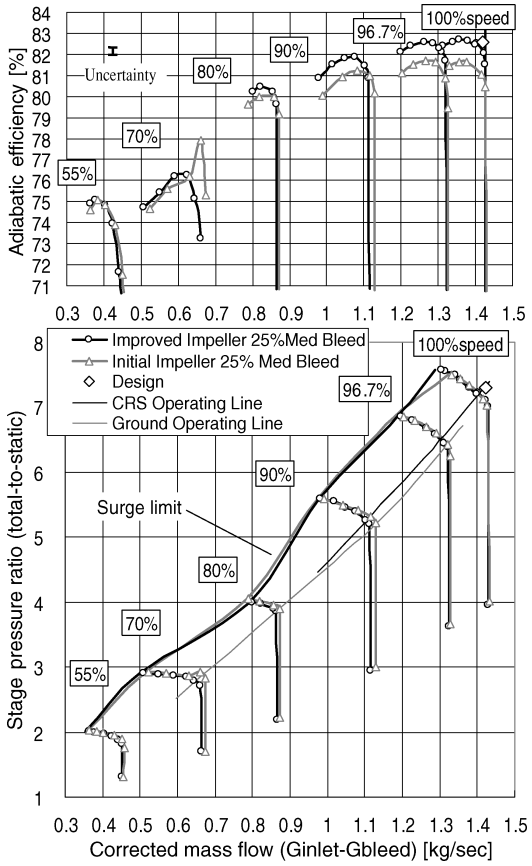

Fig. 18 Experimental stage performance map: 2.8% of bleed at design speed.

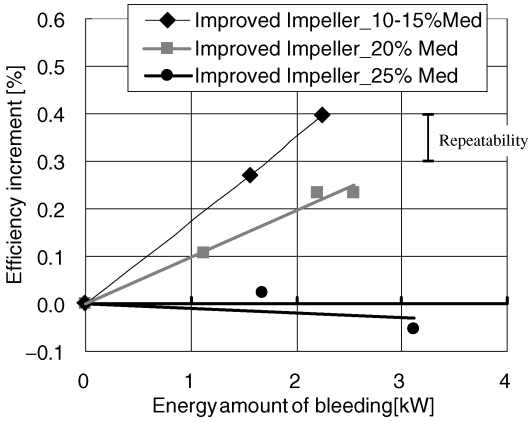

Fig. 19 Bleed effect on efficiency at design speed.

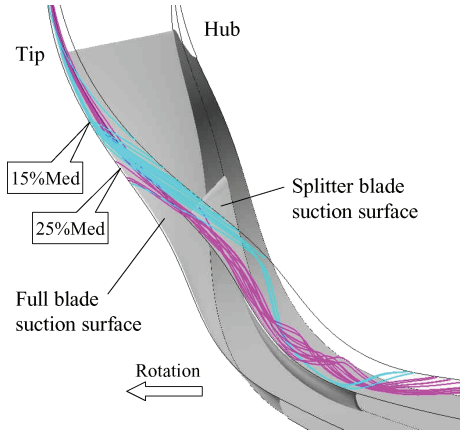

Fig. 20 Perspective view of path of CFD tracers near tip region.

out. Two meridional positions were added, 20% with a normal slot and 10–15% with inclined slot (Fig. 3).

Efficiency at Design Speed

Figure 19 shows the effect of bleed on efficiency for the improved impeller at design speed. The efficiency with bleed was obtained from a ratio of ideal-work-to-actual work including the bleed effect. Bleed position and level had a significant influence on efficiency. Figure 20 shows the reasons with the support of CFD results. There is a leakage flow in the tip region of the suction surface, at approximately 15% of meridional length. The position is also the

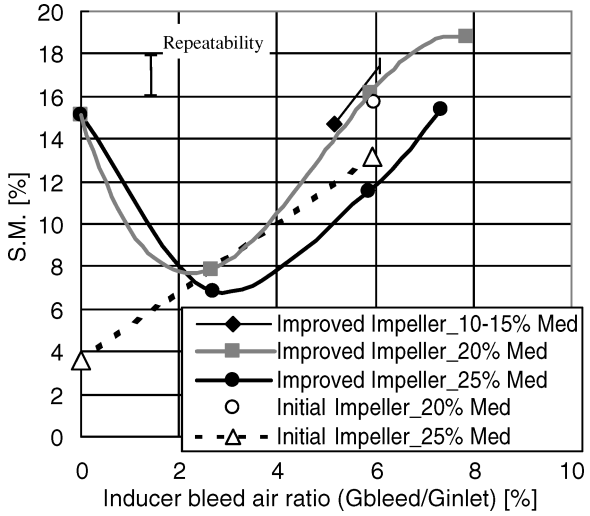

Fig. 21 Bleed effect on SM at 80% speed.

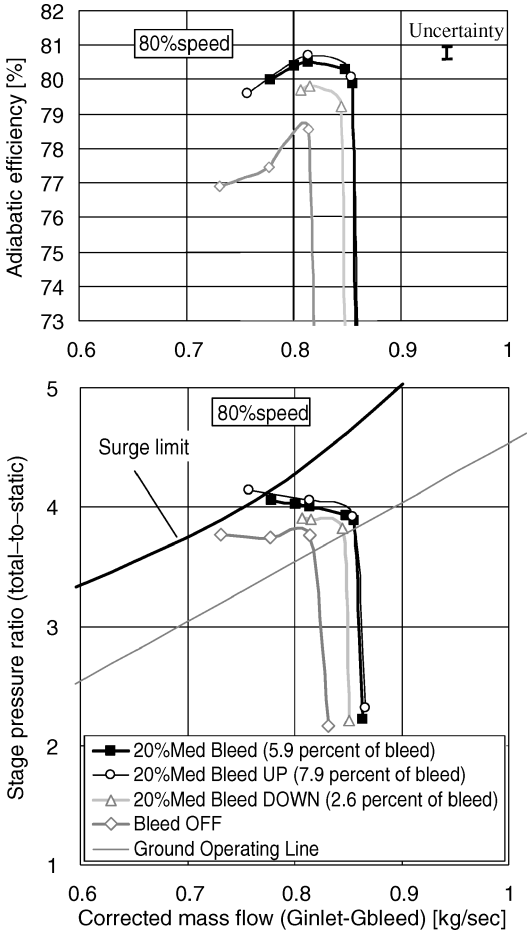

Fig. 22 Bleed effect on performance map at part speed for improved impeller.

intersection of LE shock with the SS (Fig. 6b), which explains why it is the best bleed position.

SM at Part Speed

As shown in Fig. 18, the most critical point for the SM is at 80% speed. Therefore, it was considered worthwhile to investigate the bleed characteristic in more detail. The effect of bleed level and position on SM at 80% speed is shown in Fig. 21. With respect to Fig. 21, a typical example of the performance map for the improved impeller 20%Med is shown in Fig. 22. As expected, increased SM was obtained with increased bleed air. Another optimization factor is the bleed position. In the case under consideration, the highest SM was measured with the bleed located in the range of 10–15% meridional length. However, an anomaly was observed at 0% bleed for the improved impeller. This is probably due to the improvement of inducer flowfield, but it will be an issue for future work because at the time a CFD analysis had not been conducted at 80% speed.

Conclusions

In this study, experimental and numerical investigations were carried out to provide aerodynamic guidelines for the redesign of a transonic splitter-blade impeller. An research and development program was conducted to achieve an efficiency increase of 1%. The following conclusions were drawn.

1) It was found that the definition of the blade camber surface using multiple blade sections and an independent definition of blade thickness at the SS and PS are very useful for the improvement of the flowfield.

2) Velocity peaks that were observed at the full blade LE were smoothed by modifying the spanwise distribution of LE thickness and LE wedge angle.

3) Reduction of LP was effective in suppressing three-dimensional flow.

4) An even split of the mass flow at splitter blade LE led to higher efficiency.

5) Higher bleed flows resulted in improved SM.

6) The most effective meridional bleed position was found in the area of shock wave/suction surface intersection.

Acknowledgment

The authors wish to thank Toyotaka Sonoda at Honda R&D Co., Ltd., for his support and review of the paper.

References

[1]Rodgers, C., "The Efficiency of Single Stage Centrifugal Compressors for Aircraft Applications," American Society of Mechanical Engineers, ASME Paper 91-GT-77, June 1991.

[2]Sonoda, T., Arima, T., and Oana, M., "The Effect of Inlet Boundary Layer Thickness on the Flow Within an Annular S-Shaped Duct," *Journal of Turbomachinery*, Vol. 121, No. 3, July 1999, pp. 626–634.

[3]Arima, T., Sonoda, T., Shirotori, M., Tamura, A., and Kikuchi, K., "A Numerical Investigation of Transonic Axial Compressor Rotor Flow Using a Low-Reynolds-Number k–ε Turbulence Model," *Journal of Turbomachinery*, Vol. 121, No. 1, 1999, pp. 44–58.

[4]Krain, H., "Swirling Impeller Flow," *Journal of Turbomachinery*, Vol. 110, No. 1, 1988, pp. 122–128.

[5]Arima, T., Sonoda, T., Shirotori, M., and Yamaguchi, Y., "Computation of Subsonic and Transonic Compressor Rotor Flow Taking Account of Reynolds Stress Anisotropy," American Society of Mechanical Engineers, ASME Paper, 98-GT-423, June 1998.

[6]Hah, C., and Krain, H., "Analysis of Transonic Flow Fields Inside a High Pressure Ratio Centrifugal Compressor at Design and Off Design Conditions," American Society of Mechanical Engineers, ASME-Paper, 99-GT-446, June 1999.

[7]Krain, H., Hoffmann, B., and Pak, H., "Aerodynamics of a Centrifugal Compressor Impeller with Transonic Inlet Conditions," American Society of Mechanical Engineers, ASME Paper 95-GT-79, June 1995.